ISSN 0016-7029, Geochemistry International, 2006, Vol. 44, No. 4, pp. 403–418. © Pleiades Publishing, Inc., 2006.
Original Russian Text © Yu.A. Bogdanov, A.Yu. Lein, A.M. Sagalevich, A.A. Ul'yanov, S.A. Dorofeev, N.V. Ul'yanova, 2006, published in Geokhimiya, 2006, No. 4, pp. 445–461.

Hydrothermal Sulfide Deposits of the Lucky Strike Vent Field, Mid-Atlantic Ridge

Yu. A. Bogdanov[a], A. Yu. Lein[a], A. M. Sagalevich[a], A. A. Ul'yanov[b], S. A. Dorofeev[b], and N. V. Ul'yanova[a]

[a] *Shirshov Institute of Oceanology, Russian Academy of Sciences, Nakhimovskii pr. 36, Moscow, 117997 Russia*
e-mail: lein@geo.sio.rssi.ru
[b] *Faculty of Geology, Moscow State University, Vorob'evy gory, Moscow, 119899 Russia*
e-mail: ulyanov@geol.msu.ru

Received June 24, 2004

Abstract—Several hydrothermal sulfide structures were sampled using Mir manned submersibles in the relatively shallow Lucky Strike vent field, Mid–Atlantic Ridge; the bathymetric position of these structures varies by approximately 100 m. The investigation of the chemical and mineral compositions of hydrothermal ore occurrences led to the conclusion that the initial high-temperature ore-bearing solution ascending toward the surface became unstable and experienced phase separation beneath the ocean floor. The phase separation was responsible for the bathymetric control of hydrothermal ore formation in the ocean.

DOI: 10.1134/S0016702906040070

INTRODUCTION

The systematic analysis of geological information on active hydrothermal fields in the rift zones of the Mid-Atlantic Ridge has demonstrated that the composition and properties of high-temperature hydrothermal solutions and ore occurrences are correlated with the bathymetric parameters of the hydrothermal fields. Deep-sea hydrothermal systems are accompanied by relatively high-temperature base-metal massive sulfide deposits, whereas hydrothermal sulfide ores are much less abundant at shallow sites, such as the Menez Gwen field at a depth of 871–847 m, where sulfate–anhydrite and barite occurrences are prevailing hydrothermal deposits [1]. The relatively shallow Lucky Strike vent field (depth of 1600–1700 m) is of special interest for the investigation of the bathymetric control of hydrothermal ore deposition.

The Lucky Strike vent field was discovered in 1992 during a joint French–American expedition, when samples of sulfide deposits and hydrothermal fauna were dredged. The eastern part of the field was investigated in 1993 using the manned submersible *Alvin* (six dives). During this exploration, eight active hydrothermal vents and a large area of inactive vents were discovered and sampled. In 1994 and 1997, the submarine investigations of the field were continued with the aid of manned submersibles (*Alvin* and *Nautile*). In 2002, combined oceanological studies were performed in the Lucky Strike field by the expedition of the R/V *Akademik Mstislav Keldysh* with two *Mir* submersibles.

GEOLOGIC SETTING OF THE LUCKY STRIKE FIELD

The Lucky Strike hydrothermal field is situated in the rift zone of the Mid-Atlantic Ridge, near the Azores hot spot.

The spreading ridge in this region (Fig. 1) is divided by nontransform offsets into several segments 15–80 km long. The segments show symmetrical rifts with well-defined rift valleys. The depth of the inner rift val-

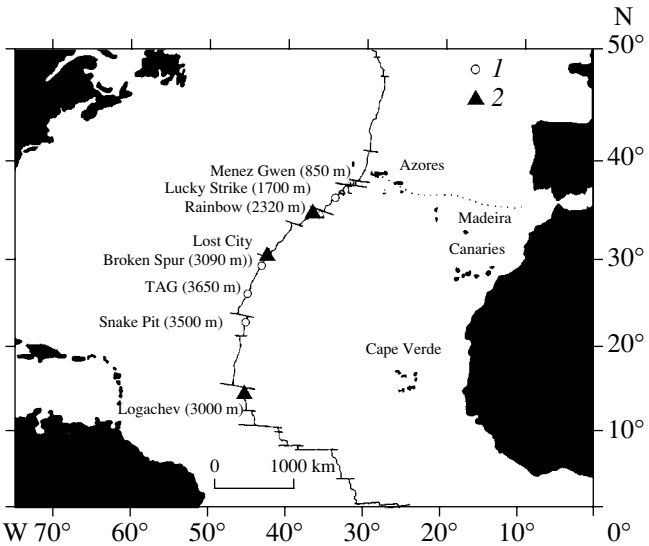

Fig. 1. Location of the Lucky Strike hydrothermal field in the rift zone of the Mid-Atlantic Ridge. Symbols show fields associated with (*1*) volcanics and (*2*) serpentinites.

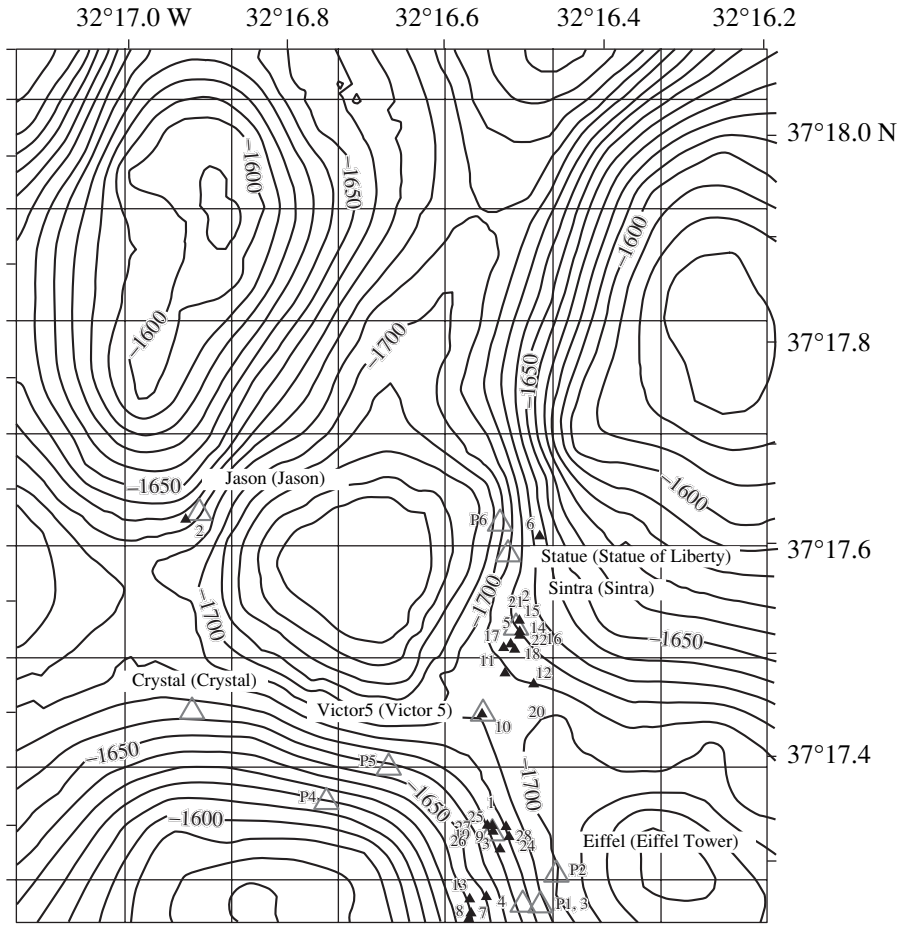

Fig. 2. Sampling sites of hydrothermal deposits during the 2002 cruise of the R/V *Akademik Mstislav Keldysh*. Isobaths are given in meters. Unfilled triangles with numbers or names are main active hydrothermal vents in various parts of the Lucky Strike field. Filled triangles are sampling sites with numbers corresponding to samples: *1*, 4376-1; *2*, 4376-2, -3, -4; *9*, 4377-4, -5; *10*, 4377-6; *11*, 4377-7; *12*, 4377-8, -9; *19*, 4383-1; *20*, 4383-2; *21*, 4383-3; *22*, 4383-4; *23*, 4383-5; and *26*, 4384-1.

ley decreases toward the triple junction near the Azores hot spot, where the rift valley practically disappears. Spreading rates are slightly different north and south of the triple junction: 25 mm/yr along an azimuth of 110° between the North American and African plates, and 27 mm/yr along an azimuth of 100° between the North American and Eurasian plates [2].

The Lucky Strike vent field lies in the rift valley of the Mid-Atlantic Ridge at 37°17′ N at depths of 1600–1730 m, within the segment of 37°–37°35′ N. The rift valley is 15 km wide there. Its central part is occupied by a volcano, which extends for 13 km along the ridge axis and has a width of 7 km and a height of 430 m [3]. The vent field occurs in a depression between three volcanic cones. Its surface is located approximately 400 m above the bottom of the rift valley (Fig. 2) [4]. The central part of the depression is a lava lake, 300 m in diameter and 6 m deep. The lake is filled with very young low-porosity lavas, whereas the volcanic cones are made up of older highly porous volcanic breccias [5].

It should be noted that the volcanic basement of the hydrothermal field is significantly enriched in incompatible elements (K, Rb, Cs, Ba, La, and Pb) compared with the most common basalts of mid-ocean ridges (N-MORB), which is attributed [6] to the influence of the Azores hot spot on the volcanism.

Hydrothermal vents are scattered over an area about 700 m across at depths from 1605 m in the north to 1730 m in the south. Some hydrothermal vents are situated on the southwestern slope of the easternmost volcanic cone forming an N–S trending chain. Other structures are situated west of the lava lake.

In this study we attempted to evaluate the influence of the bathymetric position of hydrothermal vents within the Lucky Strike active field on the mineralogical and geochemical characteristics of deposits.

MORPHOLOGY OF THE HYDROTHERMAL FIELD

The northern part of the eastern group of hydrothermal vents hosts two relatively large active structures more than 10 m in height: Statue of Liberty and Sintra. Their flanges are 10–20-cm-thick sheets extending a few meters beyond the major mound. The flanges lie directly on the basaltic basement and are overlain by complex conical structures. The lower parts of the mounds include numerous, often cemented sulfide fragments. The upper parts are composed of several low (up to 1 m) hydrothermal chimneys, some of which emanate high-temperature hydrothermal solutions to the ocean floor. Transparent and relatively low-temperature water seeps out in places on the vent slopes and from beneath the flanges. These areas are richest in bottom biota.

Low-temperature hydrothermal chert sheets with iron sulfides are widespread and relatively consistent in the southern part of the eastern chain of hydrothermal vents. The sheets pinch out in places and occasionally attain considerable thicknesses. The maximum apparent thickness of these layered sheets is 3 m. The layers contain varying proportions of silica and iron sulfides. The upper and lower surfaces of the sheets are covered by thin films of iron oxides and hydroxides. Shimmering waters were sometimes observed in the zone of sheet occurrence, where transparent warm waters flow to the surface. Mollusks and bacterial mats are abundant in such places.

There are also hydrothermal sheets, up to 10 m thick, composed of compositionally variable layers. These deposits are made up of a massive sulfide breccia cemented and locally replaced by silica and sulfides, silica and iron oxides and hydroxides, or iron and manganese oxides and hydroxides [3].

Hydrothermal vents in the southern part of the field are usually composed of small active chimneys, less than 0.5 m high and less than 10 cm in diameter, built on small (from less than 1 m to 3 m in diameter) sulfide flanges. They are typical black smokers emitting hydrothermal fluids with temperatures of 303–319°C.

The 20-m-high Eiffel Tower vent is situated in the northern part of this zone of small smokers. The temperature of its hydrothermal solutions is 325°C. The maximum temperature of hydrothermal fluid exiting at the ocean floor within the field is 333°C [7].

Zones of diffuse flow of low-temperature hydrothermal solutions are widespread in the region. They are marked by amorphous silica deposits [3].

It was pointed out [7] that young sulfide deposits usually occur on the surface of older, more weathered, and silicified breccias. The older deposits probably compose a shattered breccia flange, similar to the flanges of previously described hydrothermal vents of other fields, formed by "hydrothermal explosions."

CHEMICAL COMPOSITION OF HYDROTHERMAL DEPOSITS

The first data on the chemical composition of hydrothermal deposits from the Lucky Strike field (Table 1) were published in 1997 [6]. According to these analyses, medium-temperature Zn-rich varieties and sulfate–sulfide hydrothermal deposits are most common within the field. Higher temperature Cu-rich rocks occur in the southern part of the field.

The concentration of lead in these rocks is somewhat higher than in the high-temperature massive sulfide deposits of other oceanic hydrothermal fields. It approaches the concentration of Pb in the medium-temperature deposits of white smokers.

The major ore-forming elements of all massive sulfide and base-metal massive sulfide ore occurrences of oceanic rifts (Tables 2–5) are iron (18.04–45.1%), copper (0.03–29.4%), and zinc (0.02–9.2%). The proportions of these elements are highly variable (Fig. 3). In the three-component diagram, the fields of deposits from various hydrothermal vents overlap. However, on average, the relatively shallow northern hydrothermal vents (Sintra and Jason) show somewhat lower copper contents and higher zinc contents.

Krasnov [8] distinguished four geochemical types of massive sulfide and base-metal massive sulfide ore occurrences: massive sulfide with Cu < 4.5% and Zn < 1%; copper massive sulfide with Cu > 4.5% and Zn < 1%; zinc massive sulfide with Cu < 4.5% and Zn > 1%; and mixed copper-zinc deposits with Cu > 4.5% and Zn > 1%. Among the 23 analyses of Lucky Strike samples, copper massive sulfide ores are the most abundant (47.8%) followed by the massive sulfide (30.4%), zinc

Table 1. Chemical composition of hydrothermal deposits from the Lucky Strike field [5]

Component	Ledge	Hydrothermal chimney	
		1	2
Cu	0.31	1.14	1.95
Fe	11.44	24.1	29.1
Zn	5.63	12.95	1.71
S	24.9	36.5	38.8
SiO_2	<1	1.2	<1
Ca	0.11	<0.1	5.3
Ba	39.7	14.9	9.1
Pb	1700	505	290
Sr	8600	1900	2593
Ag	148	117	42
As	310	790	620

Note: Concentrations of components from Cu to Ba are in %, and Pb–As are in 10^{-4}%.

Table 2. Chemical composition of sulfide deposits from the Eiffel Tower vent of the Lucky Strike field

Element	I	II	III	IV	V	VI	
	4377-6	4377-4	4377-5	4384-1	4383-1	4376-1	
						a	b
Fe, %	36.23	29.9	31.51	18.81	18.04	36.4	45.1
Mn	0.027	0.012	0.012	0.001	0.058	<0.001	<0.001
Cu	2.82	29.44	5.05	14.09	7.76	6.78	2.11
Zn	0.534	0.101	0.19	0.183	8.6	0.093	0.097
Pb	0.051	0.022	0.038	<0.01	0.051	0.057	0.04
Ni	0.014	0.012	0.014	0.021	0.01	0.01	0.01
Co	0.0236	0.0265	0.0308	0.01	0.0112	0.0352	0.021
V	0.016	0.03	0.014	0.026	0.006	0.022	0.042
Cd, 10^{-4} %	35	3	6	33	502	10	3
Cr	32	20	40	34	16	40	22
Li	<4	<4	<4	4	4	<4	4
Sr, %	0.01	0.078	0.01	0.092	0.016	0.012	0.0276
Ca	0.0289	0.0632	0.0289	0.0692	0.0546	0.0226	0.0768
Mg	0.002	0.048	0.002	0.0202	0.0202	0.0384	0.0384
Al	0.24	0.128	0.024	0.272	0.468	0.234	0.064
Ti	<0.01	<0.01	<0.01	<0.01	0.104	<0.01	<0.01

Note: I–V, fragments of massive sulfide deposits from the slope of the vent; VI, a fragment of a hydrothermal chimney recovered from the flange at the base of the vent: (a) loose material from the central part and (b) massive material from the outer part.

Table 3. Chemical composition of sulfide deposits from the Sintra vent of the Lucky Strike field

Element	I		II	III	IV	V	VI	VII	IX	X
	4377-10		4379-2	4383-3	4383-4	4383-6	4383-7	4383-2	4377-8	4377-9
	2	4								
Fe, %	38.58	37.32	36.23	32.6	33.69	23.8	31.51	18.8	24.8	27.6
Mn	0.04	0.024	0.169	0.005	0.006	0.015	0.033	0.022	0.001	<0.001
Cu	4.52	8.79	3.38	6.93	6.03	15.29	4.07	0.566	2.82	16.48
Zn	0.414	0.292	0.094	0.234	0.02	0.023	0.037	7.5	0.092	0.052
Pb	0.072	0.048	0.048	0.036	0.024	<0.01	<0.01	0.066	0.042	0.045
Ni	0.014	0.02	0.016	0.014	0.024	0.022	0.014	0.013	0.017	0.006
Co	0.0134	0.0102	0.0265	0.0396	0.0188	0.0188	0.02	0.0081	0.0481	0.014
V	0.01	0.054	0.048	0.018	0.03	0.042	0.036	0.042	0.0148	0.011
Cd, 10^{-4} %	26	43	20	29	27	20	22	650	64	20
Cr	28	23	32	14	22	40	8	20	38	29
Li	6	4	10	6	<4	6	4	4	4	<4
Sr, %	0.017	0.016	0.0122	0.013	0.004	0.004	0.006	0.22	0.007	0.004
Ca	0.112	0.112	0.292	0.132	0.0268	0.0368	0.0756	0.104	0.066	0.0198
Mg	0.0568	0.04	0.081	0.0658	0.0192	0.0192	0.0476	0.0688	0.032	0.012
Al	0.128	0.528	0.228	0.546	0.168	0.442	0.52	0.229	0.026	<0.01
Ti	<0.01	0.0105	<0.01	0.018	<0.01	<0.01	<0.01	<0.01	<0.01	<0.01

Note: I, active chimney atop the vent: (2) main loose mass and (4) massive material from the central part; II–VI, massive deposits from the slope of the vent; and VII–X, fragments of relict chimneys collected at the base of the vent.

Table 4. Chemical composition of sulfide deposits from an unnamed hydrothermal vent near the Jason vent of the Lucky Strike field

Element	I		II	III
	4376-2		4376-3	4376-4
	2	3		
Fe, %	31.51	42.92	32.6	19.58
Mn	0.008	0.006	0.035	0.038
Cu	1.66	0.122	7.53	0.1
Zn	1.46	0.712	1.76	9.2
Pb	0.04	0.061	0.051	0.068
Ni	0.011	0.011	0.011	0.008
Co	0.019	0.0014	0.044	0.0057
V	0.018	0.022	0.018	0.034
Cd, 10^{-4} %	44	27	63	566
Cr	25	34	28	20
Li	<4	<4	4	<4
Sr, %	0.18	0.106	0.09	0.16
Ca	0.0756	0.112	0.258	0.12
Mg	0.011	0.0192	0.0842	0.0101
Al	0.05	0.012	0.286	<0.01
Ti	<0.01	0.07	<0.01	<0.01

Note: I, active hydrothermal chimney: (2) groundmass and (3) channel incrusted by large crystals; II and III, fragments of inactive chimneys collected from a talus on the vent slope.

Table 5. Chemical composition of sulfide deposits from the hydrothermal vents of the Lucky Strike field

Element	I	II	
	4379-1	4377-7	
		1	2
Fe, %	3.27	28.39	26.39
Mn	<0.001	0.038	0.027
Cu	1.89	5.1	1.89
Zn	0.059	0.346	0.223
Pb	0.01	0.041	0.04
Ni	0.013	0.01	0.012
Co	0.0004	0.0298	0.0265
V	0.048	0.016	0.019
Cd, 10^{-4} %	3	28	30
Cr	26	29	26
Li	12	4	4
Sr, %	0.22	0.006	0.0156
Ca	22.96	0.0372	0.0328
Mg	0.1257	0.013	0.0967
Al	0.026	0.244	0.462
Ti	<0.01	<0.01	<0.01

Note: I, active edifice south of the Eiffel Tower vent and II, hydrothermal chimney of an extinct vent situated between the Eiffel Tower and Sintra vents: (1) loose material from the central zone and (2) outer zone.

massive sulfide (13.0%), and mixed (8.7%) geochemical types of ore occurrence.

As to the concentrations of other chemical elements, the hydrothermal deposits of the Lucky Strike field are not much different from deposits in other deep-sea fields of the Mid-Atlantic Ridge. High lead content is mainly typical of low-temperature barite-rich rocks [6].

MINERALOGY OF HYDROTHERMAL DEPOSITS

The mineralogy of the hydrothermal deposits was investigated using samples from the surface of three active hydrothermal vents: Sintra, Eiffel Tower, and Jason, and one extinct vent sitting between active ones. The characteristics of the samples are given in Table 6.

The Sintra collection includes samples from an active hydrothermal chimney on the top of the vent (sample 4377-10) and samples from its slopes and base representing fragments of extinct chimneys (samples 4383-2 and 4377-9), a relict diffuser (sample 4383-5), and massive deposits (samples 4383-4 and 4383-3).

The active chimney shows a lateral zoning. Its outer zone is composed of a loose material with a porous structure and a fine-grained texture consisting of colloform and fine-grained marcasite with minor pyrite (Fig. 4). The pores, voids, and cavities are coated by octahedral pyrite crystals (Fig. 4a) and large platy and sometimes elongated marcasite grains (Fig. 4b). Xenomorphic aggregates of fine-grained chalcopyrite in a marcasite–pyrite groundmass appear near the central zone (healed conduit).

The central zone (conduit) is composed of intergrown medium-grained marcasite and chalcopyrite crystals. The walls of some cavities are covered by reniform chalcopyrite incrustations, and the voids are filled by large crystals (Fig. 4c). Covellite was found in the outer zones of xenomorphic chalcopyrite aggregates.

Exsolution structures developing in the chalcopyrite–sphalerite solid solution as inclusions of chalcopyrite in sphalerite were found in the groundmass. Sphalerite often forms anhedral grains in the marcasite–pyrite matrix and reniform aggregates in small voids (Figs. 4e, 4f).

Gangue minerals are represented by anhydrite with small sulfide inclusions forming layers, lenses, and veinlets. The anhydrite of lenses and veinlets is less contaminated by sulfides. Calcite was found in rare fractures. Barite is widespread, especially in reniform sphalerite aggregates (Figs. 5a, 5b). The latest low-temperature association includes opal and other minerals.

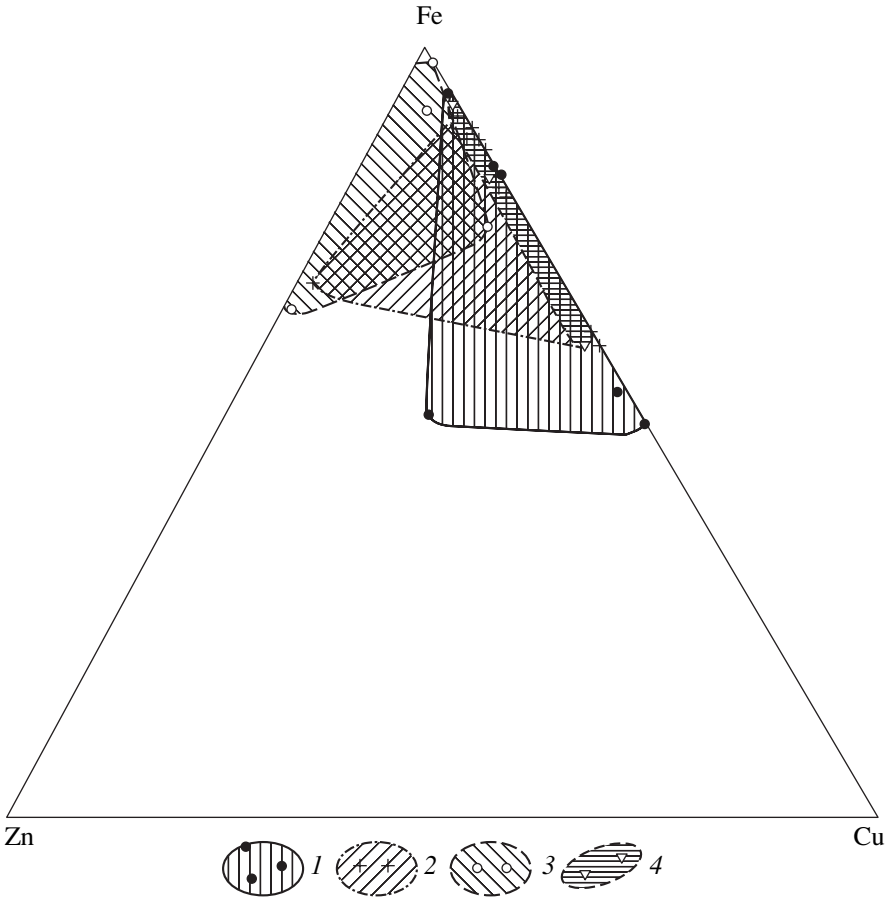

Fig. 3. Relationships of major sulfide-forming metals in the hydrothermal deposits of the Lucky Strike field. (*1*) Eiffel Tower vent, (*2*) Sintra vent; (*3*) Jason vent, and (*4*) other vents.

The surface of barite crystals is sometimes peppered with opal (Fig. 5c).

The mineral compositions of hydrothermal deposits in active and extinct structures from the slopes and base of the Sintra vent are in general similar to each other but show some differences. One inactive chimney (sample 4377-9) consisting of the chalcopyrite–marcasite–pyrite association with minor admixtures of gangue minerals was probably generated by a relatively high-temperature hydrothermal solution. Another extinct chimney (sample 4383-2) consisting of pyrite, marcasite, sphalerite, and gangue minerals (barite and silica) was formed from a low- and medium-temperature solution. It is supposed that the sulfate–massive sulfide chimneys (sample 4377-8), including no less than 30% gangue minerals, were deposited from an even colder solution.

The mineralogical analysis of samples from the Sintra vent suggested the following sequence of mineral deposition: pyrite I and marcasite I of groundmass (possibly after pyrrhotite); marcasite II, pyrite II, and chalcopyrite I; filling of conduits and cavities with pyrite III, marcasite III, and chalcopyrite II; sphalerite, chalcopyrite III (exsolution product from solid solution in sphalerite), barite, and silica.

The collection of the Eiffel Tower vent (Table 6) includes a fragment of an inactive chimney covered by mussels (sample 4384-1) sampled at the base of the structure in the shrimming water zone (Fig. 6), a fragment of an inactive chimney from the flange (sample 4376-1), and several samples of sulfide ore fragments from the vent slope (samples 4377-4-6 and 4383-1).

The hydrothermal chimney (sample 4384-1) is 30 cm in diameter and consists of several intergrown thin pipes composed of fine- and medium-grained marcasite, pyrite, and chalcopyrite. Covellite, fine-grained calcite, and native sulfur were detected on the surface of the chimney after the removal of bacterial overgrowth, slime, and mussel shells (Fig. 6). Tetrahedral sphalerite crystals with opal mantles characteristic of low-temperature deposits occur in some voids in the ore (Fig. 7a). Most voids on the chimney surface are filled with barite and opal (Figs. 7b, 7c). Sprinkling of silica minerals was observed on the crystals of pyrite (Fig. 7d) and chalcopyrite (Fig. 7e).

Of special interest are fine acicular forms (Fig. 8a) appearing as articulate aggregates at higher magnifica-

Table 6. Characteristics of samples from the hydrothermal deposits of the Lucky Strike field

No.	Sample no.	Sampling depth, m	Location in the vent	Short description	Minerals	
					major	minor
				Active vent of Sintra		
1	4383-2	1630	talus at the base	fragment of sulfide chimney	marcasite, sphalerite, barite	chalcopyrite, pyrite, calcite, opal
2	4377-9	1622	slope	fragment of sulfide chimney	chalcopyrite, marcasite	sphalerite, covellite, pyrite, barite
3	4377- 8	1616	top	active chimney consisting of several pipes with mussel druses and bacterial mats	chalcopyrite, marcasite	sphalerite, pyrite, barite, Fe hydroxides, opal
4	4383-5	1611	top	fragment of diffuser	pyrite, marcasite, sphalerite	covellite, chalcopyrite, calcite
5	4383-4	1608	talus on the slope	massive ore	pyrite, chalcopyrite	atacamite, sphalerite, marcasite, opal, barite
6	4383-3	1605	talus on the slope	massive ore	pyrite, chalcopyrite, marcasite	sphalerite, calcite, opal
				Active vent of Eiffel Tower		
7	4383-1	1678	talus at the base	massive ore	pyrite, chalcopyrite, sphalerite	covellite, calcite, barite
8	4376-1	–	talus at the base	fragment of a zoned chimney	pyrite, marcasite, chalcopyrite	sphalerite, opal, sulfates
9	4377-4	1686	talus at the base	massive ore	chalcopyrite, marcasite	sphalerite, pyrite, opal, barite
10	4377-5	1689	talus at the base	chimney with a strongly oxidized surface	marcasite, chalcopyrite	pyrite, sulfates, Fe hydroxides, opal
11	4377-6	1656	talus on the slope	massive ore	marcasite, chalcopyrite	pyrite, sphalerite, barite, opal
12	4384-1	1688	talus at the base	chimney consisting of small pipes with a mussel druse	marcasite, chalcopyrite	sphalerite, native sulfur, barite, gypsum, calcite, pyrrhotite
				Relict vent between the Sintra and Eiffel Tower vents		
13	4377-7	1645	top	chimney fragment	marcasite, chalcopyrite	pyrite, sphalerite, covellite, gangue minerals
				Unnamed active vent near the Jason vent		
14	4376-2	–	top	active chimney	chalcopyrite, marcasite, sphalerite	barite
15	4376-3	–	talus	chimney fragments	marcasite	covellite, pyrite, chalcopyrite, gangue minerals
16	4376-4	–	vent base	chimney fragment	pyrite, marcasite, sphalerite	gangue minerals

tion (Figs. 8b, 8c), which develop in microbial mats and/or mussel byssus during silicification. Such aggregates of silica minerals were reported previously, but they were observed for the first time in a sample of ore recovered directly from the shrimming water zone with all the benthos community of this environment.

The aggregates of fine-grained calcite and native sulfur (sulfurite) detected on the chimney surface are probably related to the activity of microorganisms in the outflow zone of warm hydrothermal solution.

The chalcopyrite–marcasite–pyrite association composing the hydrothermal chimney characterizes the main stage of vent formation. Hydrothermal deposits from an extinct chimney at the flange of the structure (sample 4376-1) have a very different mineral composition. This chimney also shows a concentrically zoned structure. However, its central part is composed of loose fine-grained marcasite and chalcopyrite, and the more consolidated outer wall is dominated by massive sulfides, sometimes with reniform aggregates of micro-

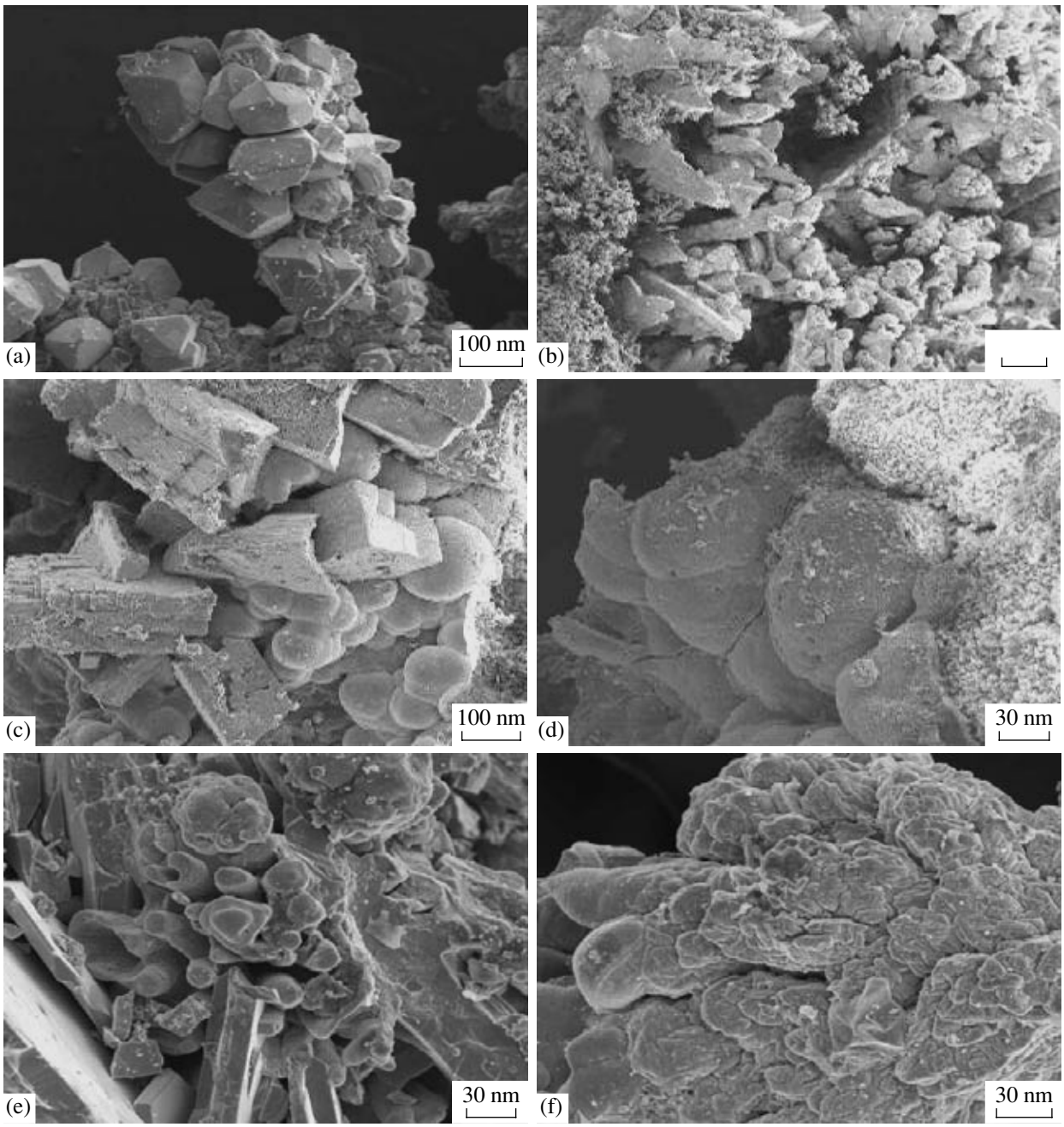

Fig. 4. Morphology of sulfide minerals in the fine- and medium-grained marcasite–pyrite groundmass from the hydrothermal deposits of the Lucky Strike field (Camscan, LINR-AN 10 000; Moscow State University). Sintra hydrothermal vent: (a) octahedral pyrite crystals (sample 4377-8); (b) elongated marcasite crystals (sample 4377-9/2); (c) reniform aggregates and prismatic crystals of chalcopyrite (sample 4383-6); and (d) colloform aggregates of chalcopyrite. Jason hydrothermal vent: (e) reniform sphalerite aggregates (sample 4376-4/2) and (f) isomorphic and reniform aggregates of sphalerite (sample 4376-4/2).

scopic chalcopyrite grains on pyrite and marcasite crystals (Fig. 7f). The voids and fractures are healed by pyrite and marcasite.

The only sample of zinc–copper massive sulfide ore (sample 4383-1) was recovered from a talus apron at the base of the Eiffel Tower vent. A fine-grained chalcopyrite–marcasite–pyrite groundmass contains irregular aggregates of colloform and occasionally fine-grained sphalerite, which was deposited relatively late together with barite and silica minerals. The latter occur as a sprinkling and crusts on practically all minerals, which suggests a late input of low-temperature silica-rich solutions.

The Jason vent collection includes a fragment of an active hydrothermal chimney (sample 4376-2) and fragments of inactive chimneys from a talus on the slope of the vent (samples 4376-3 and 4376-4). The active chimney is composed of a massive sulfide ore

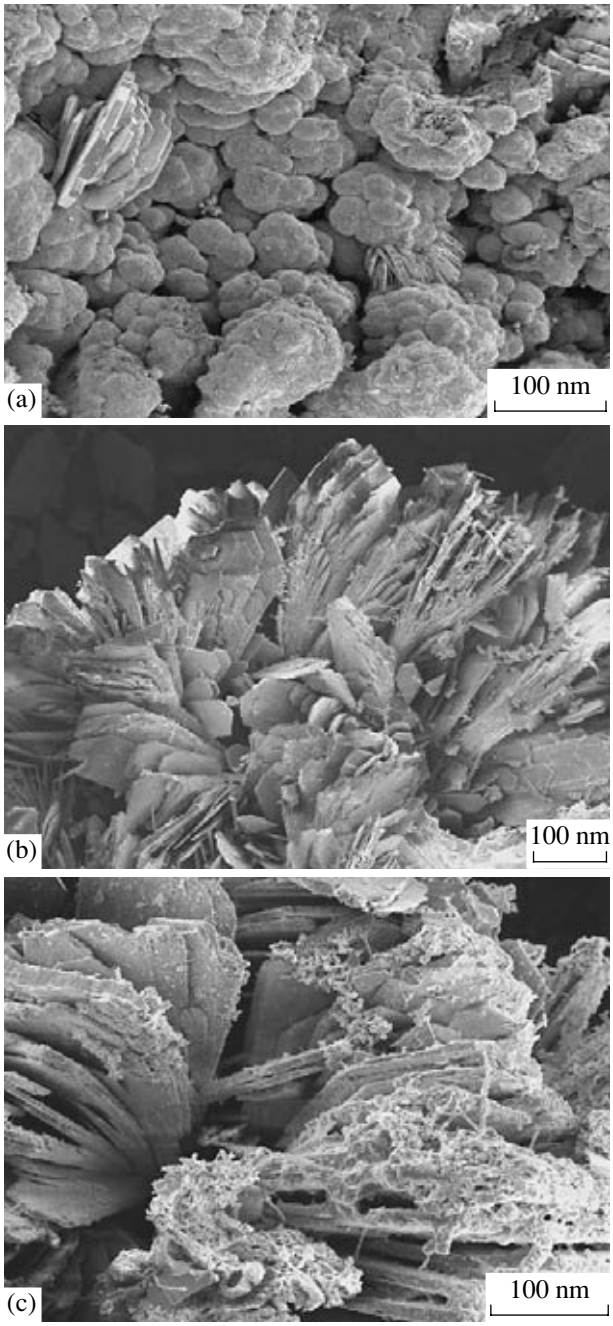

Fig. 5. Morphology of barite aggregates in the hydrothermal deposits of the Sintra vent. (a) Platy barite crystals in reniform sphalerite aggregates (sample 4377-2); (b) druse of barite crystals (sample 4383-2); and (c) opal grains on barite crystals (sample 4383-2).

with minor amounts of chalcopyrite and sphalerite in a fine-grained groundmass. The conduit of the chimney is incrusted by pyrite and marcasite crystals without other minerals.

The two extinct chimneys, one of which consists of fine-grained pyrite, marcasite, and chalcopyrite (sample 4376-3), and the other, of marcasite, sphalerite, and

Fig. 6. Surface of a sulfide pipe covered by mussels (sample 4384-1) from the discharge zone of warm solution at the base of the Eiffel Tower active vent. Light spots are occurrences of elemental sulfur (sulfurite) with dispersed fine-grained calcite.

gangue minerals (sample 4376-4), are mineralogically very similar to the sulfide chimneys of Eiffel Tower (sample 4376-1) and Sintra (sample 4383-2), respectively. Reniform sphalerite aggregates in a medium-grained pyrite–marcasite groundmass are common in the hydrothermal deposits of the Jason vent.

The chemical compositions of minerals from the hydrothermal deposits of the Lucky Strike field are given in Tables 7 and 8.

Iron disulfides (pyrite and marcasite) from the deposits of the Sintra vent contain up to 1 wt % Cu and 0.3 wt % Mn. The concentrations of Zn, Ag, As, Ni, Co, and Sb are lower than 0.02 wt %. Marcasite from the Eiffel Tower vent contains less Cu (no more than 0.6 wt %) but more Zn (up to 6.9 wt %), Mn (up to 0.6 wt %), and Co (up to 0.3 wt %). The abundances of other metals (Ag, As, Ni, and Sb) are lower than 0.02 wt %, similar to marcasite from the Sintra vent. The lowest Cu content (less than 0.2 wt %) was obtained for pyrite crystals from voids in the deposits of the Jason vent.

Chalcopyrite from the deposits of the Sintra vent contains less than 0.04 wt % Zn, less than 0.03 wt % Ni, and less than 0.02 wt % of other metals. Chalcopyrite from the Eiffel Tower vent is richer in Zn (up to 0.7 wt %), as well as in Ag, Mn, Co, and Sb (above the detection limits).

Sphalerite from the Eiffel Tower and Sintra vents contains from 2.3 to 5.4 wt % Fe and from 0.8 to 1.4 wt % Cu. The Ag content is lower than 0.3 wt % but somewhat higher than in other minerals studied. The concentration of Cd and Co in the sphalerite is up to 1.2 and 0.04 wt %, respectively.

Barite contains up to 0.22 wt % SrO, up to 0.04 wt % FeO, and up to 0.04 wt % CuO. Up to 0.11 wt % MgO were analyzed in calcite. Opal contains up to 0.05 wt %

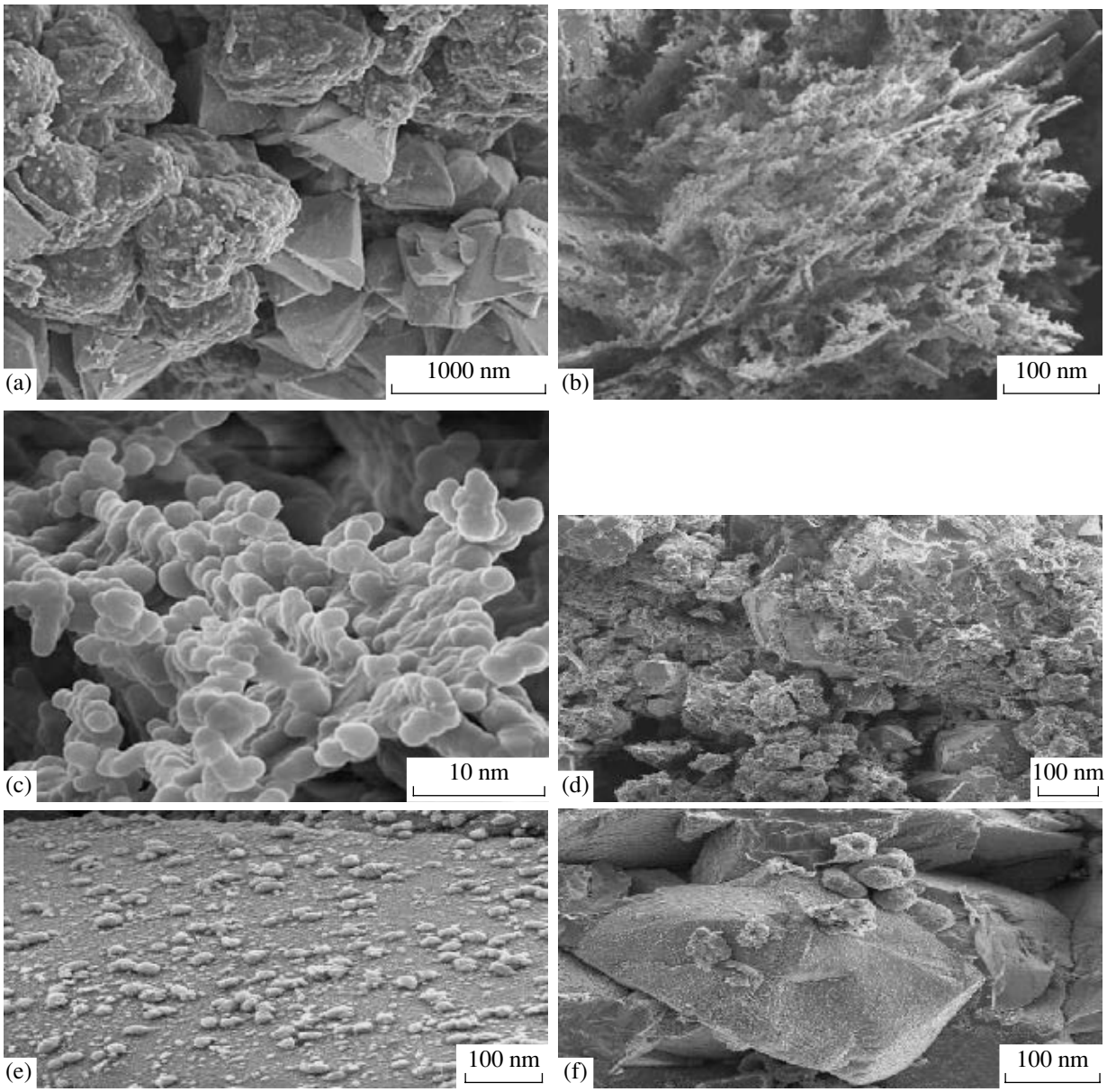

Fig. 7. Morphology of sulfide minerals and opal in samples from the active hydrothermal vent of Eiffel Tower. (a) Tetrahedral sphalerite crystals in voids with opal crusts on the surface (sample 4384-1d); (b) acicular opal aggregates (sample 4384-1b); (c) fine structure of the acicular opal aggregates (sample 4384-1b); (d) octahedral and cubic pyrite crystals with opal mantles (sample 4376-1/3); (e) face of a chalcopyrite crystal with silica sprinkling (sample 4377-5/3); and (f) pyrite grains and reniform chalcopyrite aggregates (sample 4377-5/3).

CaO, 0.43–0.77 wt % FeO, up to 0.19 wt % CuO, and up to 0.17 wt % ZnO.

The mineralogical analysis of hydrothermal deposits from the Lucky Strike field showed that the deeper Eiffel Tower vent (1678 m) is characterized by more pronounced high-temperature copper massive sulfide mineralization and much less abundant medium- and low-temperature gangue mineral assemblages, compared with the shallower Sintra vent (1605 m). It is important to emphasize that the chemical compositions of sulfide minerals from the deposits of these two vents are also different.

SULFUR ISOTOPES IN HYDROTHERMAL DEPOSITS

Sulfur isotopes were analyzed in 17 samples of sulfide deposits from the Lucky Strike field (Table 9). The $\delta^{34}S$ values of pyrite I from the hydrothermal chimneys of Eiffel Tower (–2.4‰) and Sintra (0.9‰) are most similar to the isotopic composition of the basalts.

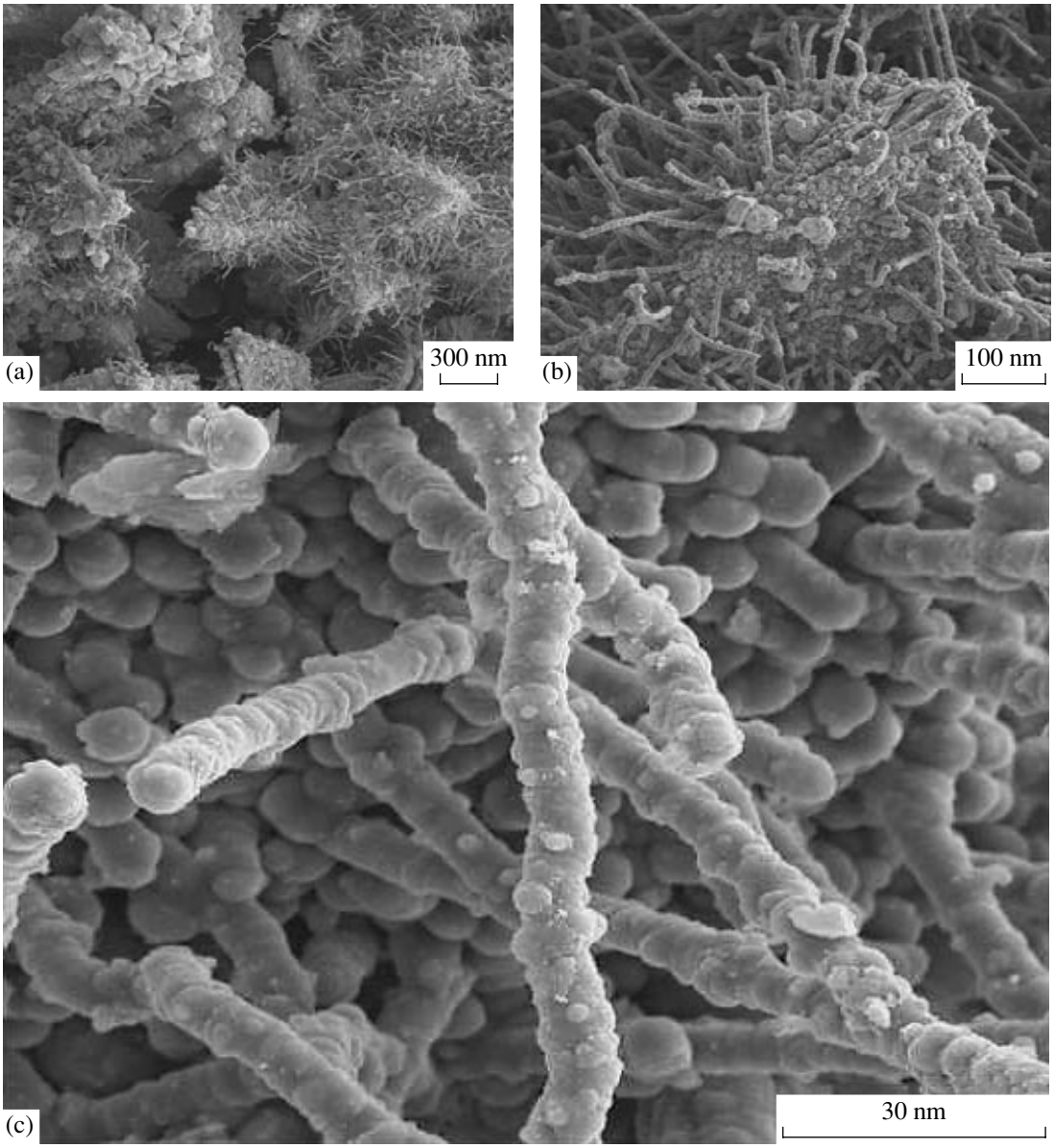

Fig. 8. Morphology of opal on the surface of a sulfide chimney from the shimmering water zone (sample 4384-1d). (a) General view of aggregates; (b) and (c) the same aggregates at a higher magnification, presumably mussel byssus overgrown by silica.

Sphalerite from the two vents shows identical sulfur isotopic compositions ($\delta^{34}S$ of 3.4 and 3.5‰).

On the other hand, the major minerals of the copper massive sulfide deposits of the Eiffel Tower vent are slightly depleted (by 1‰ on average) in ^{34}S compared with pyrite and chalcopyrite from the hydrothermal deposits of Sintra. Crystals of later pyrite from incrustations in pores and voids are isotopically heavier than fine-grained pyrite from the groundmass. A significant difference in sulfur isotopic composition between sulfides and native sulfur is probably related to microbial processes occurring under the participation of sulfate ions from ambient seawater. The contribution of microbial sulfur to the formation of barite in both vents is even more pronounced.

The authors accept the model of hydrothermal solution formation as a result of interaction between seawater penetrating into the crust and basalts at the roof of a magma chamber (reaction zone). The oceanic water loses the major portion of sulfate ions already in the descending limb of the circulation system during migration into the reaction zone.

The analysis of the data suggests that sulfur from the country basalts entrained into the hydrothermal solution is the major source of sulfide sulfur during the formation of hydrothermal deposits in both vents. However, a slightly higher $\delta^{34}S$ value in pyrite and chalcopy-

Table 7. Chemical compositions of ore minerals from the hydrothermal vents of the Lucky Strike field

No.	Sample	Fe	Cu	As	S	Ni	Co	Cd	Sb	Mn	Zn	Ag	Total
						Eiffel Tower							
						Marcasite							
1	4383-M1-1	46.73	0.03	b.d.l.	54.47	b.d.l.	0.08	n.d.	b.d.l.	b.d.l.	0.02	0.05	101.32
2	4384-M2-1d	46.45	0.23	b.d.l.	53.42	b.d.l.	0.06	n.d.	b.d.l.	b.d.l.	0.12	b.d.l.	100.28
3	4384-M2-1d	46.38	0.64	b.d.l.	53.41	b.d.l.	0.04	n.d.	b.d.l.	0.04	0.15	b.d.l.	100.67
4	4377-M2-7/1	43.51	0.52	b.d.l.	53.54	b.d.l.	0.05	n.d.	b.d.l.	0.59	0.43	b.d.l.	98.63
5	4377-M2-7/1	45.45	0.61	b.d.l.	53.53	b.d.l.	0.27	n.d.	b.d.l.	b.d.l.	0.22	b.d.l.	100.07
6	4377-M2-7/1	46.91	b.d.l.	0.06	53.02	b.d.l.	0.12	n.d.	b.d.l.	b.d.l.	b.d.l.	b.d.l.	100.11
7	4377-M2-7/1	46.45	0.03	b.d.l.	54.00	0.05	b.d.l.	n.d.	b.d.l.	0.02	b.d.l.	b.d.l.	100.56
8	4383-M1-7	44.54	0.11	b.d.l.	53.70	b.d.l.	0.10	n.d.	b.d.l.	0.47	b.d.l.	b.d.l.	98.91
						Chalcopyrite							
1	4384-M2-1d	29.53	33.78	b.d.l.	36.02	b.d.l.	0.02	n.d.	b.d.l.	0.02	0.14	0.11	99.50
2	4384-M2-1d	29.91	33.61	b.d.l.	34.71	b.d.l.	0.02	n.d.	b.d.l.	b.d.l.	0.04	0.05	98.29
3	4384-M2-1d	30.20	34.51	b.d.l.	35.02	b.d.l.	b.d.l.	n.d.	b.d.l.	b.d.l.	0.13	b.d.l.	99.87
4	4383-M1-1	30.05	34.64	b.d.l.	34.47	b.d.l.	b.d.l.	n.d.	0.02	0.03	b.d.l.	b.d.l.	99.21
						Covellite							
1	4383-M1-7	0.59	63.90	b.d.l.	34.03	b.d.l.	b.d.l.	n.d.	b.d.l.	b.d.l.	0.02	b.d.l.	98.54
2	4383-M1-3(5)	1.99	64.25	b.d.l.	33.55	b.d.l.	b.d.l.	n.d.	b.d.l.	b.d.l.	0.04	0.03	99.83
3	4383-M1-3(5)	0.51	65.23	b.d.l.	33.70	b.d.l.	b.d.l.	n.d.	b.d.l.	0.02	0.08	0.06	99.54
						Sphalerite							
1	4384-M2-1d	5.38	1.32	n.d.	33.54	n.d.	0.04	0.28	n.d.	b.d.l.	58.13	0.35	92.33
2	4384-M2-1a	2.32	0.81	n.d.	33.05	n.d.	b.d.l.	0.18	n.d.	0.02	61.32	0.10	94.66
3	4384-M2-1a	5.78	0.84	n.d.	33.45	n.d.	0.04	0.36	n.d.	0.02	57.08	b.d.l.	90.94
4	4384-M2-1a	2.65	1.41	n.d.	32.70	n.d.	b.d.l.	1.21	n.d.	b.d.l.	59.75	0.06	93.72
						Pyrrhotite							
1	4384-M2-1e	59.44	0.41	n.d.	39.25	n.d.	b.d.l.	n.d.	n.d.	b.d.l.	b.d.l.	b.d.l.	99.11
2	4384-M2-1e	58.48	2.27	n.d.	39.21	n.d.	0.11	n.d.	n.d.	0.09	b.d.l.	0.08	100.26
3	4384-M2-1e	59.58	0.02	n.d.	38.56	n.d.	b.d.l.	n.d.	n.d.	b.d.l.	0.05	b.d.l.	98.23
No.	Sample	Fe	Cu	As	S	Ni	Co	Sb	Mn	Zn	Ag	Total	
						Sintra vent							
						Pyrite							
1	4383-M1-3/5	48.08	b.d.l.	0.07	54.86	0.04	0.11	0.04	b.d.l.	b.d.l.	b.d.l.	103.21	
2	4383-M1-3(a)	47.69	b.d.l.	b.d.l.	53.33	b.d.l.	0.01	b.d.l.	b.d.l.	b.d.l.	b.d.l.	101.03	
3	4383-M1-3(a)	47.47	0.25	b.d.l.	52.67	0.02	0.06	b.d.l.	b.d.l.	b.d.l.	b.d.l.	100.46	
4	4383-M1-3(5)	47.30	0.25	0.09	53.68	b.d.l.	b.d.l.	b.d.l.	b.d.l.	b.d.l.	b.d.l.	101.31	
5	4383-M1-3/5	46.83	0.06	b.d.l.	53.69	0.03	0.06	0.03	b.d.l.	b.d.l.	b.d.l.	100.70	
6	4383-M1-3(a)	46.74	0.14	0.17	52.87	b.d.l.	0.08	0.03	b.d.l.	b.d.l.	b.d.l.	100.04	
7	4383-M1-3/5	46.51	0.12	0.13	54.13	0.02	0.05	b.d.l.	b.d.l.	b.d.l.	b.d.l.	100.96	
8	4383-M1-7	46.46	0.07	b.d.l.	53.71	0.06	0.03	0.05	b.d.l.	b.d.l.	b.d.l.	100.38	
9	4383-M1-7	46.44	0.15	b.d.l.	53.69	b.d.l.	0.06	b.d.l.	b.d.l.	b.d.l.	b.d.l.	100.34	
10	4383-M1-7	46.12	b.d.l.	b.d.l.	54.18	b.d.l.	0.11	b.d.l.	0.03	b.d.l.	b.d.l.	100.43	
11	4383-M1-7	45.86	1.05	0.06	52.70	b.d.l.	0.03	b.d.l.	0.02	b.d.l.	b.d.l.	99.72	
						Chalcopyrite							
1	4384-M2-1d	30.39	33.58	b.d.l.	35.53	b.d.l.	b.d.l.	b.d.l.	b.d.l.	0.04	b.d.l.	99.54	
2	4384-M2-1d	30.20	33.86	b.d.l.	35.44	b.d.l.	b.d.l.	b.d.l.	b.d.l.	0.04	0.06	99.54	
3	4384-M2-1d	30.11	34.16	b.d.l.	34.55	b.d.l.	0.04	b.d.l.	0.03	b.d.l.	b.d.l.	98.88	
4	4384-M2-1d	30.10	34.39	b.d.l.	34.99	b.d.l.	0.03	0.02	0.04	b.d.l.	b.d.l.	99.55	
5	4384-M2-1d	30.09	34.76	b.d.l.	34.29	0.03	0.07	b.d.l.	b.d.l.	b.d.l.	b.d.l.	99.25	

Note: b.d.l.—below detection limit and n.d.—not determined.

Table 8. Chemical compositions of gangue minerals from the Sintra vent

Mineral	Sample	CaO	BaO	SrO	MgO	FeO	NiO	CoO	MnO	CuO	ZnO	SO_3	ClO	SiO_2	Total
Barite	4383-M1-4	0.28	54.72	0.22	b.d.l.	0.00	b.d.l.	0.05	b.d.l.	0.00	b.d.l.	29.70	b.d.l.	b.d.l.	84.98
Opal	4383-M1-4	b.d.l.	0.03	0.12	0.03	0.37	b.d.l.	b.d.l.	b.d.l.	0.18	0.16	0.15	0.14	90.19	91.40
Opal	4383-M1-4	b.d.l.	0.02	0.17	b.d.l.	0.60	b.d.l.	b.d.l.	b.d.l.	0.03	b.d.l.	0.02	0.03	91.70	92.59
Opal	4383-M1-4	0.04	b.d.l.	0.06	0.05	0.57	b.d.l.	b.d.l.	0.05	0.18	b.d.l.	0.08	0.10	92.66	93.78
Barite	4383-M1-4	0.03	69.14	0.08	b.d.l.	0.04	b.d.l.	b.d.l.	b.d.l.	0.04	b.d.l.	34.23	0.02	b.d.l.	103.60
Calcite	4383-M1-5 I	43.75	0.02	0.19	3.95	0.05	b.d.l.	b.d.l.	b.d.l.	b.d.l.	b.d.l.	0.49	0.02	b.d.l.	48.48
Calcite	4383-M1-5 I	44.36	0.06	0.18	3.90	0.07	b.d.l.	b.d.l.	b.d.l.	0.08	b.d.l.	0.56	b.d.l.	b.d.l.	49.24
Calcite	4383-M1-5 I	46.23	b.d.l.	0.21	3.47	0.06	b.d.l.	b.d.l.	b.d.l.	b.d.l.	0.05	0.50	0.04	b.d.l.	50.58
Calcite	4383-M1-5 I	47.11	0.09	0.12	2.16	0.41	b.d.l.	b.d.l.	b.d.l.	b.d.l.	0.13	0.55	b.d.l.	0.05	50.62

Table 9. Isotopic compositions of sulfur for the hydrothermal deposits of the Lucky Strike field

No.	Sample no.	Mineral	$\delta^{34}S$, ‰	Sample description
			Sintra vent	
1	4377-10a	pyrite	2.1	young chimney atop the vent, loose outer zone
2	4377-10b	pyrite (chalcopyrite)	0.9	same chimney, massive inner zone
3	4377-8	pyrite (chalcopyrite)	3.0	sulfide chimney from talus at the base of the vent
4	4377-9	pyrite (chalcopyrite)	3.8	chimney on the slope
5	4383-2a	sphalerite	3.5	chimney at the base
6	4383-2b	chalcopyrite	3.7	same place
7	4383-7a	pyrite	3.6	massive ore from the slope
8	4383-7b	barite	16.0	same ore, druses in voids
			Eiffel Tower vent	
9	4376-1a	pyrite	–2.4	chimney fragment at the flange of the event, loose central zone
10	4376-1b	pyrite (chalcopyrite)	1.3	massive outer zone of chimney
11	4377-4	pyrite (chalcopyrite)	2.3	massive ore, fragment from the slope
12	4377-5	pyrite (chalcopyrite)	2.5	same
13	4377-6	pyrite	2.7	same
14	4383-1a	sphalerite	3.4	same
15	4383-1b	pyrite (chalcopyrite)	2.3	same
16	4384-1	pyrite	1.4	chimney fragment with a mussel druse at a warm solution outlet
17	4384-1a	pyrite (chalcopyrite)	1.7	same place
18	4384-1b	large pyrite crystals	3.9	same place, incrustations in pores
19	4384-1c	native sulfur	5.6	same place, aggregates of sulfurite (bacterial) sulfur on the surface of sample
20	4384-1d	barite	12.7	same place, druses in voids

rite from the shallower Sintra vent compared with the Eiffel Tower vent deserves special attention. If the hydrothermal deposits of the field are formed from a single hydrothermal solution, it experiences at shallower depths a certain influence of new portions of seawater penetrating into the crust, and sulfate ions from seawater are reduced to sulfide ions, which shifts the sulfur isotopic composition of sulfides.

DISCUSSION

The first results obtained for the Lucky Strike vent field associated with basalts revealed both a striking similarity and significant differences between the compositions of hydrothermal deposits from this field and from other hydrothermal sites of oceanic rifts. Compared with massive sulfide and base-metal massive sulfide ore occurrences from deeper fields of oceanic rifts, hydrothermal deposits from some vents of the Lucky Strike field are strongly enriched in barium and, occasionally, in lead. This is a characteristic feature of many relatively shallow fields formed in various geodynamic settings, including the Menez Gwen field in the Mid-Atlantic Ridge [3], the Endeavor segment [9] and Axial seamount [10] of the Juan de Fuca Ridge, Franklin seamount of the Woodlark basin in the western Pacific [11], seamounts of the Izu–Bonin volcanic arc [12], the Sumisu back-arc rift of the Izu–Bonin arc [13], and many others.

The reason for the development of such a peculiar structure of hydrothermal deposits can be determined from information on the composition and properties of the hydrothermal solutions from which these deposits were formed [4–6]. Compared with other known fields of the Mid-Atlantic Ridge, these solutions are characterized by higher pH values; lower contents of Fe, Mn, Li, and Zn; and higher contents of Ba, K, Cs, and Rb. Their chloride contents are equal or lower (by up to 20%) than that of ambient seawater. The total gas content, except for H_2S and He, is three times that of the TAG field, and the methane content is 7–10 times that of the Snake Pit field.

Based on the systematization of investigations of hydrothermal solutions from the Lucky Strike field, Von Damm et al. [5] concluded that the primary hydrothermal solution of this site was formed in a reaction zone through interaction between oceanic water and oceanic crustal rocks at a pressure of about 300 bar, i.e., about 1300 m below the ocean floor, and at a temperature of about 400°C. The oceanic water reacts with an altered, relatively oxidized substrate [5]. The hydrothermal solution reaching the bottom surface probably experienced supercritical phase separation already in the oceanic crust. It should be pointed out that phase separation of ascending high-temperature hydrothermal solutions within the oceanic crust was reliably established in some of the aforementioned shallow hydrothermal fields where compositionally similar hydrothermal deposits occur. The enrichment of hydrothermal solutions in Ba, K, Cs, and Rb can be due to the elevated contents of these elements in the basalts, which is related to the influence of the Azores hot spot.

The different temperatures and compositions of hydrothermal solutions from various hydrothermal springs of the field are explained by variable mixing proportions between the light freshened fluid ascending to the surface (after phase separation) and seawater [4, 5].

The fact that the colder solutions show lower gas abundances than the hotter solutions [6] indicates that a heavy salt phase may contribute to the mixture. Thus, it can be supposed that variations in the composition and properties of the hydrothermal solutions at Lucky Strike are related to mixing between three components: light and heavy phases formed by phase separation and seawater. The depletion of the hydrothermal solutions in metals compared with the solutions from deeper vent fields indicates a minor contribution from the heavy phase, which usually concentrates metals during phase separation.

The Lucky Strike field is situated at depths (1618–1730 m) where phase separation occurs, which affects the composition and properties of hydrothermal solutions and hydrothermal deposits.

We believe that the primary high-temperature ore-bearing hydrothermal solution is formed at the roof of a crustal magma chamber through seawater–basalt interaction. During its ascent to the ocean floor, the solution may become unstable at a certain depth and experience phase separation in response to a decrease in hydrostatic pressure. Direct measurements in hydrothermal fields and experiments showed that metals partition into the high-salinity heavy phase, whereas gases are accumulated in the freshened low-density phase [14–17]. Part of the metals, primarily those forming higher temperature mineral assemblages, may be precipitated as vein and stockwork mineralization. The low content of metals in the hydrothermal solutions of Lucky Strike is an indicator of preliminary phase separation.

The presence among the hydrothermal occurrences of the field of both high-temperature copper-rich and lower temperature barite deposits suggests that the Lucky Strike field represents only the initial stages of the influence of phase separation on the composition of hydrothermal deposits at depths of 1618–1730 m. In the Menez Gwen vent field, which is located to the north of Lucky Strike at depths of 847–871 m, this phase separation affected the compositions and properties of both hydrothermal solutions and hydrothermal deposits. The hydrothermal deposits of the Menez Gwen field are dominated by sulfate (anhydrite and barite) types with disseminated sulfides.

The bathymetric control of ore deposition is responsible for the compositional difference between the hydrothermal deposits of vents located at depths between 500 and 1000 m.

Some comments can be made concerning the age of the Lucky Strike hydrothermal field. Unfortunately, there are still no direct isotopic determinations of the age of hydrothermal deposits, and only some indirect evidence exists. First of all, many of the studied hydrothermal vents, including relict ones, have practically no

sedimentary cover. Some of them are built up directly on the volcanic basement, which is also not covered by sediments. Even the low-temperature hydrothermal sheets are only locally sprinkled with unconsolidated sediments.

It should be noted that the rates of sedimentation estimated in this region by the investigation of bottom sedimentary columns recovered directly near two neighboring hydrothermal fields, Lucky Strike and Menez Gwen, are relatively high, 3–30 cm per one thousand years [18]. The distribution of sedimentary cover suggests that the hydrothermal deposits of the Lucky Strike field can be only slightly older than 1 ka, and are probably younger.

Another way of estimating the age of a hydrothermal field is based on the analysis of the morphology of hydrothermal edifices. Bogdanov et al. [19] presented a sequence of growth of a hydrothermal deposit. During the initial stage, lasting no more than one thousand years (Broken Spur stage), isolated hydrothermal vents are formed directly on the surface of the volcanic basement. Basement volcanics occupy considerable areas of ocean floor between them. By the end of the second stage with the maximum age of 4000 yr (Snake Pit stage), the flanges of individual vents begin to coalesce into a single structure. Individual vents develop above this common flange. In our opinion, the morphology of the Lucky Strike hydrothermal field is transitional between these two stages and closer to the former.

It is worth noting that Richter [18] described a sedimentary column with an age of no more than 30 ka recovered about 20 km south of the Lucky Strike hydrothermal field, which contained several intervals characterized by very high accumulation rates of "hydrothermal" chemical elements (Fe, Mn, Cu, and Zn) in the sediments [18]. This discrepancy with our estimates can be explained either by the contribution of hydrothermal elements from another source occurring south of the Lucky Strike field or supposing that some preexisting hydrothermal vents of the field were buried by volcanic eruptions. The hydrothermal activity connected with the observed hydrothermal vents lasts for slightly more than 1000 yr.

CONCLUSIONS

The relatively shallow Lucky Strike field in the Mid-Atlantic Ridge includes several individual vents differing in bathymetric depth by about 100 m and showing distinctive compositions and properties of hydrothermal ores. This is related to the instability and phase separation of ascending high-temperature ore-bearing solution beneath the ocean floor. The data obtained are important for the description of the variability of ore deposition under conditions of phase separation, which is responsible for the bathymetric control of hydrothermal ore accumulation in the ocean.

ACKNOWLEDGMENTS

The samples used in this study were obtained during expeditions of the R/V *Akademik Mstislav Keldysh* with the manned submersible *Mir*. The laboratory investigations were financially supported in part by the Russian Foundation for Basic Research, project nos. 03-05-64346 and 03-05-64414.

REFERENCES

1. Yu. A. Bogdanov, *Hydrothermal Occurrences in Rifts of the Mid-Atlantic Ridge* (Nauchnyi Mir, Moscow, 1997) [in Russian].
2. R. S. Detrick, P. Buhl, J. Mutter, et al., "Multichannel Seismic Imaging of a Crustal Magma Chamber along the East Pacific Rise," Nature **326**, 35–41 (1987).
3. Y. Fouquet, J.-L. Charlou, I. Costa, et al., "A Detailed Study of the Lucky Strike Hydrothermal Site and Discovery of a New Hydrothermal Site: Menez Gwen; Preliminary Results of the DIVA 1 Cruise (5–29 May, 1994)," InterRidge News **3** (2), 14–17 (1994).
4. J. L. Charlou, I. P. Donval, E. Douville, et al., "Compared Geochemical Signatures and the Evolution of Menez Gwen (37°50′ S) and Lucky Strike (37°17′ S) Hydrothermal Fields, South of the Azores Triple Junction on the Mid-Atlantic Ridge," Chem. Geol. **171**, 49–75 (2000).
5. K. L. von Damm, A. M. Bray, L. G. Buttermore, and S. E. Oosting, "The Geochemical Controls on Vent-Fluids from the Lucky Strike Vent Field, Mid-Atlantic Ridge," Earth Planet. Sci. Lett. **160**, 521–536 (1998).
6. C. Langmuir, S. Humphris, D. Fornary, et al., "Hydrothermal Vents at 37° N on the Mid-Atlantic Ridge," Earth Planet. Sci. Lett. **148**, 69–91 (1997).
7. S. E. Humphris and Lucky Strike Team, "Comparison of Hydrothermal Deposits at Lucky Strike Vent Field with Other Mid-Ocean Ridge Vent Sites," EOS Trans. AGU **74**, 100 (1993).
8. *Hydrothermal Sulfide Ores and Metalliferous Sediments of the Ocean,* Ed. by I. S Gramberg and A. I. Ainemer (Nedra, St. Petersburg, 1992) [in Russian].
9. D. Stakes and W. W. Moore, "Evolution of Hydrothermal Activity on the Endeavour–Juan de Fuca Ridges: Observations, Mineral Ages, and Ra Isotope Ratios," J. Geophys. Res. **97**, 21 739–21 752 (1991).
10. *Geological Structure and Hydrothermal Rocks of the Juan de Fuca Ridge*, Ed. by A. P. Lisitsyn (Nauka, Moscow, 1990) [in Russian].
11. A. P. Lisitsyn, R. A. Binns, Yu. A. Bogdanov, et al., "Modern Hydrothermal Activity of Franklin Seamount, Western Part of the Woodlark Basin, Papua–New Guinea," Izv. Akad. Nauk SSSR, Ser. Geol., No. 8, 125–140 (1991).
12. G. P. Glasby, K. Lizasa, M. Yuasa, and F. Usui, "Submarine Hydrothermal Mineralization on the Izu–Bonin Arc, South of Japan: An Overview," Mar. Geores. Geotechnol. **18**, 141–176 (2000).

13. T. Urabe and M. Kusakabe, "Barite Silica Chimneys from the Sumisu Rift, Izu–Bonin Arc: Possible Analog to Hematitic Chert Associated with Kuroko Deposits," Earth Planet. Sci. Lett. **100**, 283–290 (1990).

14. S. G. Krasnov, "Minimum Depths of Pyrite Ore Formation at the Ocean Floor," Dokl. Akad. Nauk SSSR **296**, 1188–1191 (1987).

15. T. Finlow-Bates and D. E. Large, "Water Depth as Major Control on the Formation of Submarine Exhalative Ore Deposits," Geol. Jb. **D30**, 2739 (1978).

16. J. L. Bischoff and R. J. Rosenbauer, "Liquid–Vapor Relation in the Critical Region of the System NaCl–H_2O from 380 to 415°C: A Refined Determination of the Critical Point and Two-Phase Boundary of Seawater," Geochim. Cosmochim. Acta **52**, 2121–2126 (1988).

17. J. L. Bischoff and R. J. Rosenbauer, "Phase Separation in Seafloor Geothermal System: An Experimental Study of the Effects on Metal Transport," Am. J. Sci. **287**, 953–978 (1987).

18. T. Richter, "Sedimentary Fluxes at the Mid-Atlantic Ridge," Doctoral Dissertation. Geomar. Report **73** (Geomar, Kiel, 1998).

19. Yu. A. Bogdanov, N. S. Bortnikov, and A. P. Lisitsyn, "The Origin of the Hydrothermal Sulfide Ores in the Axial Parts of the Mid-Atlantic Ridge," Geol. Rudn. Mestorozhd. **39**, 409–429 (1997) [Geol. Ore Dep. **39**, 351 (1997).